Geochemistry, Geophysics, Geosystems®

RESEARCH ARTICLE
10.1029/2025GC012683

3-D Modeling of Differential Exhumation of Ultrahigh-Pressure Metamorphic Rocks Driven by Increasing Plate Divergence

Xinxin Wang[1], Liang Zhao[1,2], Marco G. Malusà[3], Weiqiang Ji[1], and Jie Yuan[1]

[1]State Key Laboratory of Lithospheric and Environmental Coevolution, Institute of Geology and Geophysics, Chinese Academy of Sciences, Beijing, China, [2]College of Earth and Planetary Sciences, University of Chinese Academy of Sciences, Beijing, China, [3]Department of Earth and Environmental Sciences, University of Milano-Bicocca, Milano, Italy

Abstract Petrological and seismic constraints suggest differential sampling depth for ultrahigh pressure (UHP) metamorphic rocks exposed in different segments of the fossil subduction zone of the Western Alps. However, the mechanisms for the observed differential exhumation remain to be understood. Here, we account for the continental margin subduction within double subduction systems coupled with three-dimensional (3-D) geodynamic models to investigate the potential for this phenomenon. We tested two end-member scenarios of upper-plate motion, including Adria counterclockwise rotation and divergent motion away from the trench. Results show that both scenarios can produce a unidirectional increase in the metamorphic peak of exhumed UHP rocks along the orogen strike. Only in the simulations where the counterclockwise rotation of the upper plate acts as the primary driver of exhumation did the resulting characteristics of the deep structure fit with those observed in the Western Alps. They include the presence of an exhumed mantle wedge beneath the southern UHP domes and its absence beneath the northern UHP domes. Our results can be exported to other subduction zones where kinematic constraints suggest a component of upper-plate rotation, such as eastern Papua New Guinea, and to older subduction zones where the kinematics is poorly assessed.

Plain Language Summary The Western Alps have undergone the continental-margin burial and exhumation of UHP rocks, providing crucial insights into the Earth's interior. Recent seismic and petrological experiments identified distinct metamorphic peaks of exhumed UHP rocks throughout the Western Alps. However, numerical models used so far to test these processes are primarily 2-D, despite the fact that the Western Alps have a strongly variable tectonic structure in 3-D. In this study, we used 3-D numerical models tailored to the Western Alps natural laboratory, and found that Adria counterclockwise rotation can induce the presence of an exhumed mantle wedge beneath the southern UHP domes, while its absence is observed beneath the northern UHP domes. Consequently, the resulting metamorphic peak of exhumed UHP rocks increases along the orogen strike, which aligns with observations in the Western Alps. We argue that increasing plate divergence caused by upper plate rotation can explain the lateral variation in pressure peaks observed in many UHP terranes where the kinematics are no longer ascertainable.

Key Points:

- The differential exhumation of UHP metamorphic rocks is numerically investigated using 3-D models
- Exhumed UHP rocks and the mantle wedge exhibit changes along the orogen strike
- The features produced by upper-plate counterclockwise rotation fit with those in the Western Alps

Supporting Information:

Supporting Information may be found in the online version of this article.

Correspondence to:

L. Zhao,
zhaoliang@mail.iggcas.ac.cn

Citation:

Wang, X., Zhao, L., Malusà, M. G., Ji, W., & Yuan, J. (2026). 3-D modeling of differential exhumation of ultrahigh-pressure metamorphic rocks driven by increasing plate divergence. *Geochemistry, Geophysics, Geosystems*, *27*, e2025GC012683. https://doi.org/10.1029/2025GC012683

Received 18 SEP 2025
Accepted 18 FEB 2026

Author Contributions:

Conceptualization: Xinxin Wang, Liang Zhao
Formal analysis: Xinxin Wang, Liang Zhao
Funding acquisition: Liang Zhao
Investigation: Xinxin Wang, Liang Zhao, Marco G. Malusà, Weiqiang Ji, Jie Yuan
Methodology: Xinxin Wang
Visualization: Xinxin Wang
Writing – original draft: Xinxin Wang
Writing – review & editing: Xinxin Wang, Liang Zhao, Marco G. Malusà, Weiqiang Ji

1. Introduction

The Western Alps are one of the best-preserved subduction wedges in the world and thereby offer an unparalleled opportunity for investigating processes leading to exhumation of UHP rocks (e.g., Agard, 2021; Guillot et al., 2009). Their deep structure has been revealed by high-resolution seismic experiments (Malusà et al., 2021; Solarino et al., 2024; Zhao et al., 2015, 2020). The discovery of coesite-bearing eclogite in the Dora-Maira dome (Chopin, 1984) has provided the first petrological evidence for continental subduction and exhumation and has been replicated in several locations of the so-called Eocene eclogite belt (Figure 1a). It is generally agreed that UHP metamorphic peaks vary along strike (Figure 1b and Table 1), with the greatest sampling depths observed in rocks exposed in the Dora-Maira dome (Rubatto & Hermann, 2001). Moreover, an exhumed mantle wedge has been detected beneath the Dora-Maira dome but not beneath the Gran Paradiso dome in the northern Western Alps (Solarino et al., 2024), showing that UHP rock exhumation must be understood in 3-D.

Various mechanisms that are proposed for distinct exhumation of UHP rocks in the Alpine subduction zone, include channel flow (synconvergent-induced exhumation; e.g., Butler et al., 2013; Vaughan-Hammon et al., 2021; Yamato et al., 2008), slab breakoff (Davies & von Blanckenburg, 1995; Duretz & Gerya, 2013),

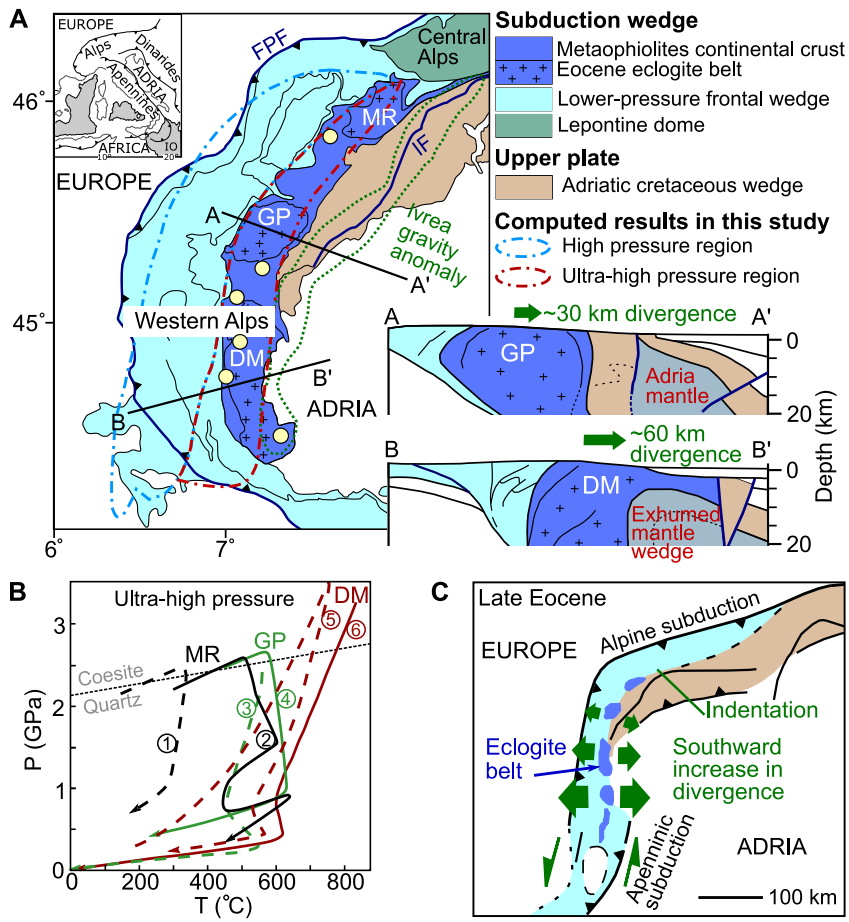

Figure 1. Geological and petrological setting. (a) Simplified geological map of the Western Alps and crustal cross sections along the CIFALPS profiles (acronyms: DM, Dora-Maira; GP, Gran Paradiso; MR, Monte Rosa; FPF, Frontal Pennine Fault; IF, Insubric Fault; Malusà et al., 2015; Solarino et al., 2024). Yellow circles represent the localities with coesite-bearing rocks in the Eocene eclogite belt (Chopin, 1984; Ghignone et al., 2023, 2024; Maffeis et al., 2025; Manzotti et al., 2022; Reinecke, 1991). (b) Representative *P-T-t* paths of exhumed UHP rocks: 1—Le Bayon et al. (2006), 2—Gasco et al. (2011), 3 and 6—Malusà et al. (2011), 4—Gasco et al. (2010), 5—Rubatto and Hermann (2001). (c) Palinspastic reconstruction of the Alpine belt in the late Eocene (after Solarino et al., 2024).

slab rollback (Brun & Faccenna, 2008; Husson et al., 2010) and upper-plate divergent motion (e.g., Liao et al., 2018; Malusà et al., 2011, 2015). They have revealed that the plate convergence and subduction channel weakening are effective for controlling the burial depth and exhumation of continental-margin crust, respectively.

Table 1
Observed Peak Pressure-Temperature of Metamorphic Rocks for Three Different HP-UHP Tectonic Units in the Western Alps Mentioned in This Study

HP-UHP tectonic units from north to south in the Western Alps	Peak pressure (GPa)	Peak temperature (°C)	References	Figure and label
Monte Rosa	2.4	475–535	Le Bayon et al. (2006)	Figure 1b and ①
	2.4–2.7	550–570	Gasco et al. (2011)	Figure 1b and ②
	2.0–2.4	540–600	Luisier et al. (2019)	–
	1.4–1.8	565–605	Vaughan-Hammon et al. (2021)	–
Gran Paradiso	2.4	560	Malusà et al. (2011)	Figure 1b and ③
	2.6–2.7	580–600	Gasco et al. (2010)	Figure 1b and ④
Dora-Maira	3.5	700–750	Rubatto and Hermann (2001)	Figure 1b and ⑤
	3.2	830	Malusà et al. (2011)	Figure 1b and ⑥

The majority of these mechanisms are tested in 2-D numerical models, indicating that the peak metamorphic gradients of exhumed HP-UHP rocks rise in the direction perpendicular to the orogen strike (e.g., Liao et al., 2018). However, little is known about the physics of the differential sampling depth of exhumed UHP rocks along the orogen strike, which is an intrinsically 3-D process. Based on previous 3-D modeling of the discontinuous distribution of UHP terrane in the Western Gneiss Complex (Bottrill et al., 2014), plate rotation may provide one mechanism for differential exhumation in the Western Alps, although it is unclear how geodynamically feasible this is.

The 3-D kinematics of the Western Alps subduction system was largely determined by a big change in the relative Adria-Europe plate motion between 49 and 35 Ma (Dewey et al., 1989; Jolivet et al., 2003), potentially linked to the rotation of Adria (van Hinsbergen et al., 2014) and northwestward Apenninic subduction in the south (Figure 1c). This change led to the indentation of Adria beneath the Central Alps and to a southward increase in divergence between the upper plate and the trench along the Western Alps subduction zone. This kinematics can be modeled numerically as a counterclockwise rotation of the upper plate relative to the trench.

In this study, we employ 3-D geodynamic modeling to investigate the potential differential exhumation of UHP rocks driven by increasing plate divergence. We test two end-member scenarios of upper-plate motion, that is, Adria counterclockwise rotation and divergent motion away from the trench. We anticipate that, although both model categories successfully reproduce the pressure-temperature-time (*P-T-t*) paths observed in exhumed UHP rocks, only the Adria counterclockwise rotation model effectively simulates the differential exhumation of the mantle wedge that was imaged by recent seismic experiments (Solarino et al., 2024).

2. Geologic Setting

The Western Alps are the result of Late Cretaceous to Paleogene oblique subduction of the Alpine Tethyan ocean and adjacent European continental margin beneath the Adriatic microcontinent, and subsequent hard collision starting from the Oligocene (Dewey et al., 1989; Handy et al., 2010; Jolivet et al., 2003; Malusà et al., 2015; Zhao et al., 2016). Their southward termination was characterized by two oppositely dipping subductions, the southeastward Alpine subduction in the north and the northwestward Apenninic subduction in the south (Figure 1c). In the Alpine subduction system, UHP metamorphic rocks exposed in the Western Alps were buried and reached the eclogite peak at ∼35 Ma (Rubatto & Hermann, 2001) and later were rapidly exhumed to the Earth's surface at rates of 10–30 mm/yr by 32 Ma. Rapid exhumation was thought to be triggered by southward-increasing amounts of upper-plate divergent motion away from the Alpine trench (Malusà et al., 2015) as a consequence of the coeval indentation of the Adriatic lithosphere beneath the future Central Alps in the north (Figure 1c; Solarino et al., 2018, 2024). Meanwhile, in the Apenninic subduction system, the Apenninic slab progressively shifted northward (Malusà et al., 2015) and started interacting with the European slab by the end of the Oligocene (Malusà et al., 2016; Zhao et al., 2016). The retreat of the Apenninic slab initiated in the Neogene after the cessation of Alpine subduction (Faccenna et al., 2014).

The geologic record of UHP rock exhumation in the Western Alps orogen is preserved in full (Figure 1a). Metamorphic rocks are exposed between two major faults, the Frontal Pennine Fault on the lower-plate side of the orogen, and the Insubric Fault on the upper-plate side. This latter side shows the strongly positive Ivrea gravity anomaly (e.g., Zahorec et al., 2021), which provides evidence of mantle rocks exhumed to shallow depth. On the lower-plate side, two main tectonic domains with specific metamorphic imprint formed during Paleogene subduction and collision (Malusà et al., 2011): (a) the Eocene Eclogite belt, which is composed of UHP rock domes derived from subducted European crust (DM, GP and MR in Figure 1a), tectonically enveloped by UHP metaophiolites, such as the Zermatt-Saas and Viso metaophiolites (Ghignone et al., 2023; Manzotti et al., 2022; Rubatto & Hermann, 2001; Starr et al., 2020); and (b) a lower-pressure doubly vergent Paleogene frontal wedge, consisting of blueschist-greenschist facies units either derived from the European paleomargin or from sediments and ophiolites of the subducted Alpine Tethys (Dumont et al., 2022; Malusà et al., 2005).

3. Methods

3.1. Numerical Method

We employed the LaMEM code (Kaus et al., 2016) to generate 3-D geodynamic simulations of double subduction systems, tailored to models of the specific kinematics and tectonic settings of the Western Alps (Figure 1c). The

Table 2
Physical Properties of the Rocks Used in This Study

Phase	Rock	ρ_0 (kg/m^3)	c (MPa)	φ (°)	B_d/B_l (Pa^{-n}/s)	E_d/E_l (kJ/mol)	V_d/V_l (m^3/mol)	n	H_r (W/m^3)
Upper continental crust	Dry quartzite[a]	2750	20	30	6.7×10^{-6}/–	156/–	0/–	2.4	10^{-6}
Lower continental crust	Dry diabase[b] (Mafic granulite[a])	2900	20	30	3.2×10^{-20} (1.4×10^{4})/–	276/–	0/–	3.05 (4.2)	10^{-6}
Oceanic crust	Wet quartzite[a]	2900	1	2	3.2×10^{-4}/–	154/–	0/–	2.3	0
Mantle lithosphere	Dry olivine[c]	3300	20	30	1.1×10^{5}/1.5×10^{9}	530/375	15×10^{-6}/4×10^{-6}	3.5	0
Upper mantle	Dry olivine[c]	3300	20	30	1.1×10^{5}/1.5×10^{9}	530/375	15×10^{-6}/4×10^{-6}	3.5	0
Lower mantle	Dry olivine[c]	3300	20	30	1.1×10^{5}/1.5×10^{9}	530/375	15×10^{-6}/4×10^{-6}	3.5	0
Weak zone	Wet quartzite[a]	3300	1	1	3.2×10^{-4}/–	154/–	0/–	2.3	0
Sediment	Wet quartzite[a]	2600	20	30	3.2×10^{-4}/–	154/–	0/–	2.3	10^{-6}

[a]Rock properties: Ranalli (1995). [b]Huismans et al. (2001). [c]Hirth and Kohlstedt (2004).

governing equations for conservation of mass, momentum and energy, assuming the Boussinesq approximation and incompressible flow, can be written as:

$$\frac{\partial v_i}{\partial x_i} = 0 \tag{1}$$

$$\frac{\partial \tau_{ij}}{\partial x_j} - \frac{\partial P}{\partial x_i} + \rho g_i = 0 \tag{2}$$

$$\rho C_p \frac{DT}{Dt} = \frac{\partial}{\partial x_i}\left(k \frac{\partial T}{x_i}\right) + H_a + H_s + H_r \tag{3}$$

where v_i is the velocity, x_i ($i = 1, 2, 3$) Cartesian coordinates, τ_{ij} the deviatoric stress tensor, P the total pressure, $\rho = \rho_0(1 - \alpha(T - T_0))$ density with ρ_0 the reference density at T_0 the reference temperature and $\alpha = 3 \times 10^{-5}$ K^{-1} the thermal expansivity, g_i the gravitational acceleration, $C_p = 1000$ J/(kg*K) the heat capacity, $\frac{D}{Dt}$ the material time derivative, $k = 3.5$ W/(m*K) the thermal conductivity, and H_a, H_s, H_r are the adiabatic, shear and radioactive heating, respectively. Other employed physical properties of the different phases in this study are listed in Table 2.

For incompressible flow, the deviatoric stress tensor τ_{ij} is defined by:

$$\tau_{ij} = 2\eta_{\text{eff}} \dot{\varepsilon}_{ij} \tag{4}$$

where η_{eff} is the effective viscosity and $\dot{\varepsilon}_{ij} = \frac{1}{2}\left(\frac{\partial v_i}{\partial x_j} + \frac{\partial v_j}{\partial x_i}\right) - \frac{1}{3}\frac{\partial v_k}{\partial x_k}\delta_{ij}$ is the deviatoric strain rate tensor.

The rock rheology is assumed to be visco-elasto-plastic assuming a Maxwell body, which can be calculated as

$$\dot{\varepsilon}_{ij} = \dot{\varepsilon}_{ij}^{el} + \dot{\varepsilon}_{ij}^{vs} + \dot{\varepsilon}_{ij}^{pl} = \frac{1}{2G}\frac{D\tau_{ij}}{Dt} + \dot{\varepsilon}_{\text{II}}^{vs}\frac{\tau_{ij}}{\tau_{\text{II}}} + \dot{\varepsilon}_{\text{II}}^{pl}\frac{\tau_{ij}}{\tau_{\text{II}}} \tag{5}$$

where $\dot{\varepsilon}_{ij}^{el}$, $\dot{\varepsilon}_{ij}^{vs}$ and $\dot{\varepsilon}_{ij}^{pl}$ represent the elastic, viscous, and plastic components, respectively. $G = 40$ GPa is the elastic shear modulus. $\frac{D\tau_{ij}}{Dt} = \frac{\partial \tau_{ij}}{\partial t} + \tau_{ik}\omega_{kj} - \omega_{ik}\tau_{kj}$ denotes the Jaumann objective stress rate with $\omega_{ij} = \frac{1}{2}\left(\frac{\partial v_i}{\partial x_j} - \frac{\partial v_j}{\partial x_i}\right)$ the spin tensor. The subscript II represents the square root of the second invariant of the corresponding tensor such as the deviatoric stress $\tau_{\text{II}} = \left(\frac{1}{2}\tau_{ij}\tau_{ij}\right)^{\frac{1}{2}}$.

Viscous deformation is composed of diffusion creep ($\dot{\varepsilon}_l$) and dislocation creep ($\dot{\varepsilon}_d$):

$$\dot{\varepsilon}_{ij}^{vs} = \dot{\varepsilon}_l + \dot{\varepsilon}_d = A_l \tau_{\mathrm{II}} + A_d (\tau_{\mathrm{II}})^n \tag{6}$$

where the subscripts l and d, and the superscript n represent the corresponding parameters of diffusion creep and dislocation creep, and the stress exponent of the dislocation creep, respectively. $A_l = B_l \exp\left[\frac{-E_l + PV_L}{\mathrm{RT}}\right]$ and $A_d = B_d \exp\left[\frac{-E_d + PV_d}{\mathrm{RT}}\right]$ are the pre-exponential factor of the corresponding creep mechanism, in which B is the creep constant, E the activation energy, V the activation volume of the corresponding creep mechanism and R the gas constant.

Rocks fail in a plastic manner if the second invariant of the deviatoric stress exceeds the yield stress. $\dot{\varepsilon}_{\mathrm{II}}^{pl}$, the second invariant of the plastic strain rate tensor, is determined by enforcing the Drucker-Prager yield criterion:

$$\tau_Y = \sin(\varphi) P + \cos(\varphi) C \tag{7}$$

where φ is the friction angle, C the cohesion.

During advection, the elastic history stresses from previous time step (τ_{ij}^n) are corrected on the markers to account for the rigid-body rotation, and then interpolated on the edge and cell control volumes using the distance-based averaging to obtain the effective strain rates ($\dot{\varepsilon}_{ij}^*$):

$$\dot{\varepsilon}_{ij}^* = \dot{\varepsilon}_{ij} + \frac{\tau_{ij}^*}{G\Delta t} \tag{8}$$

where $\tau_{ij}^* = \tau_{ij}^n + \Delta t \left(\omega_{ik}\tau_{kj}^n - \tau_{ik}^n \omega_{kj}\right)$ and Δt is the model time step.

The effective viscosity η_{eff} and the updated deviatoric stresses τ_{ij} are computed from the effective strain rates, using the standard quasi-viscous expression:

$$\tau_{ij} = 2\eta_{\mathrm{eff}}\dot{\varepsilon}_{ij}^*, \eta_{\mathrm{eff}} = \min\left[\left(\frac{1}{G\Delta t} + \frac{1}{\eta_{\mathrm{creep}}}\right)^{-1}, \frac{\tau_Y}{2\dot{\varepsilon}_{\mathrm{II}}^*}\right]. \tag{9}$$

3.2. Model Setup

The initial model setup includes two oppositely dipping adjacent subduction systems (Figure 2), separated by a transform fault. In the north, the Alpine Tethys oceanic plate and the European continental margin subduct beneath the overriding Adriatic microcontinent along the Alpine trench. In the south, the Ionian oceanic plate subducts beneath the European continental margin along the Apenninic trench. The numerical model domain is $2000 \times 1500 \times 860$ km^3 in the x, y, and z directions, respectively, which is resolved with $257 \times 257 \times 129$ grid points. The highest resolution is distributed in the lithosphere and uppermost asthenosphere, which is $7.8 \times 5.6 \times 2.5$ km (in x-y-z). Both the European and Adriatic continental plates have a 35-km-thick crust, with a 20-km-thick upper crust and a 15-km-thick lower crust, whereas the crustal thickness of the oceanic plate is 10 km. The lithospheric thickness for both continental plates is set at 100 km, with the same thickness for the oceanic plate. Passive tracers are set up in the European continental-margin crust to trace and record the P-T-t paths of the exhumed rocks. They are arranged in the following directions: from 1000 km to 1250 km at 6 km intervals in the x direction, from 650 to 1000 km at 15 km intervals in the y direction, and from 0 to 40 km at 2 km intervals in the z direction (Figure 2b). Only a portion of the highlighted tracers—light blue circles that map the deformation processes of the upper crust—are displayed here. It is important to note that the pressure shown in the P-T-t paths is dynamic pressure rather than lithostatic pressure.

Thermal boundary conditions are isothermal at the top (0°C) and bottom (1590°C), with zero-heat flux applied at the side boundaries. We employ a linear temperature profile from 0°C at the surface to 1350°C at the bottom of the lithosphere, where the T_{moho} on the Adriatic microcontinent ranges from 600°C to 800°C. For the oceanic plate, a 50-Myr-old half-space thermal cooling model is employed. All the mechanical boundary conditions are set to free

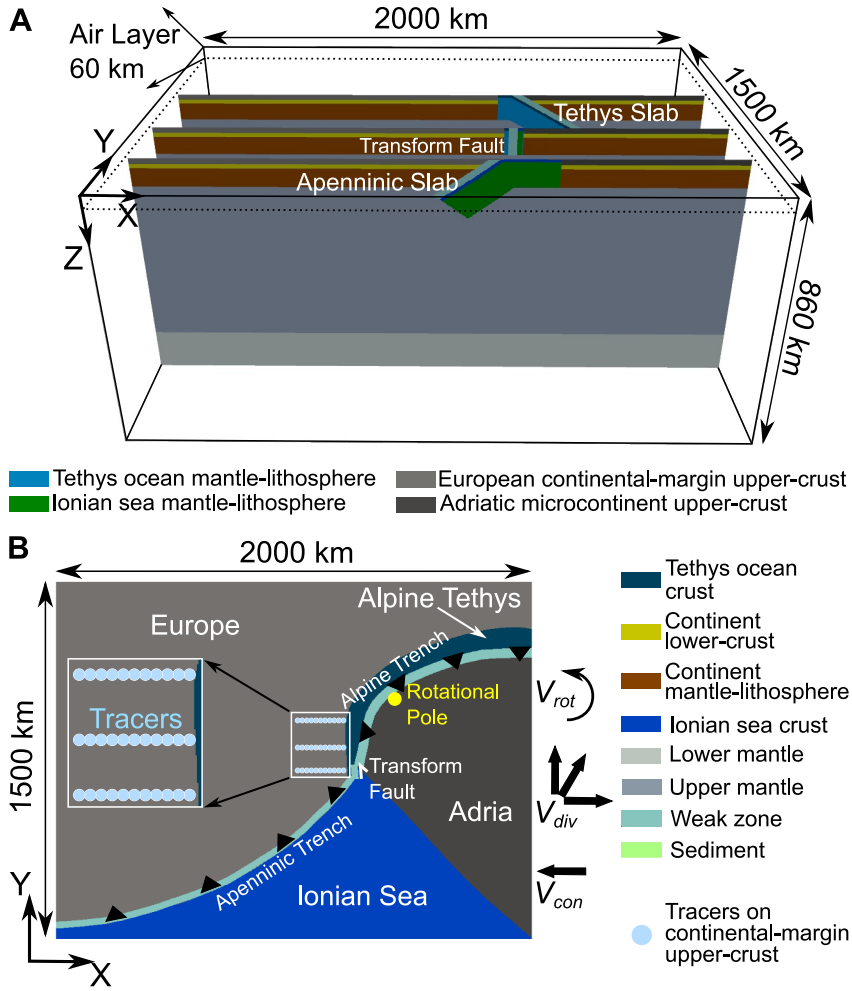

Figure 2. Initial model setup with material distribution in panel (a) 3-D perspective and (b) 2-D map views. The light blue circles indicate tracers positioned on the thinned crust of the continental margin for tracing the *P-T-t* paths. The black arrows located at the right boundary show the externally imposed convergence (V_{con}), divergence (V_{div}), and counterclockwise rotation (V_{rot}) of the Adriatic microcontinent, respectively. The yellow solid circle represents the pole of counterclockwise rotation. The black sawtooth curves and white arrow denote the initial positions of the two trenches and transform fault, respectively.

slip, and a sticky air (thickness of 60 km and viscosity of 10^{18} Pa s) is implemented on top to mimic the internal free surface (Crameri et al., 2012; Kaus et al., 2010).

We focus on the differential exhumation of UHP rocks in the Western Alps according to two different scenarios: (i) Adria rotates counterclockwise by ~5–18° at ~44-35 Ma and (ii) Adria diverges from the trench at ~49 Ma without rotation. In scenario (i), which is considered in our Reference model, the pole of counterclockwise rotation is located in the Adriatic upper plate adjacent to the Alpine trench (Figure 2b). We impose a convergence rate (V_{con}) of 40 mm/yr on the European plate during the first 8 Myr of the model evolution, followed by either a counterclockwise rotation (scenario i: rates V_{rot} vary from 0 to 6.4°/Myr) to simulate southward-increasing amounts of divergence, or a change in motion velocity (scenario ii: direction varies from westward to northward, northeastward, and eastward; rates V_{div} vary from 10 to 60 mm/yr).

4. Model Results

4.1. Reference Model Evolution

The parameter choices for different models that are designed to simulate these two scenarios, along with their corresponding results, have been summarized in Table 3. In scenario (i), differential exhumation of UHP rocks

Table 3
Parametric Settings and Computed Results Mentioned in This Study

Name of the numerical model	Adria conterclockwise rotation rate V_{rot} (°/Myr)/imposed time (Myr)	Adria divergence rate V_{div} (mm/year)/imposed time (Myr)	Adria abrupt change in motion direction	Adria Moho temperature T_{moho} (°C)	Convergence-extension transition time (Myr)	Metamorphic grade in MR/GP/DM	Occurrence of the differential exhumation	Figure
Reference model								
Reference	2.0/8-14	–	–	600	8	REUHP/REUHP/REUHP	Yes	1,3,4,6
Effect of Adria rotation rate								
MPR0	0/8-22	–	–	600	8	SEHP/SEHP/SEUHP	Yes	4
MPR05	0.5/8-22	–	–	600	8	SEUHP/SEUHP/SEUHP	Yes	4,5
MPR1	1.3/8-22	–	–	600	8	REUHP/REUHP/REUHP	Yes	-
MPR4	4.0/8-14	–	–	600	8	REUHP/REUHP/REUHP	Yes	-
MPR6	6.4/8-14	–	–	600	8	REUHP/REUHP/REUHP	Yes	4,5
Effect of Adria Moho temperature								
MMO7	2.0/8-16	–		700	8	REUHP/REUHP/REUHP	Yes	-
MMO8	2.0/8-16	–		800	8	REHP/REHP/REUHP	Yes	4,6
Effect of convergence-extension time								
MCV14	–	–		600	14	SEHP/SEHP/SEHP	Yes	4
Effect of Adria abrupt change in the divergence rate and direction								
MPD10	–	10/8-22	From west to northeast	600	8	SEHP/SEUHP/SEUHP	Yes	8
MPD30	–	30/8-14	From west to northeast	600	8	REUHP/REUHP/REUHP	Yes	7,8
MPD60	–	60/8-14	From west to northeast	600	8	REUHP/REUHP/REUHP	Yes	8
MDC90	–	26/8-14	From west to north	600	8	SEHP/SEUHP/SEUHP	Yes	8
MDC180	–	15/8-14	From west to east	600	8	REUHP/REUHP/REUHP	Yes	7,8
Combined effect of Adria rotation and abrupt change in motion								
MR4D2	2.0/8-12	30/12-14	To northeast	600	8	REUHP/REUHP/REUHP	Yes	7,8
MR2D4	2.0/8-10	30/10-14	To northeast	600	8	REUHP/REUHP/REUHP	Yes	–
MD2R4	2.0/10-14	30/8-10	From west to northeast	600	8	REUHP/REUHP/REUHP	Yes	–
MD4R2	2.0/12-14	30/8-12	From west to northeast	600	8	REUHP/REUHP/REUHP	Yes	–

Note. Acronyms: DM, Dora-Maira; GP, Gran Paradiso; MR, Monte Rosa; REUHP, rapid exhumation of UHP rocks; REHP, rapid exhumation of HP rocks; SEUHP, slow exhumation of UHP rocks; SEHP, slow exhumation of HP rocks.

was obtained in the Reference model with Adria counterclockwise rotation of 2.0°/Myr. As the model progressed, the continental margin subducts and reaches a maximum depth of ∼120 km in the northern vertical profile (AA′) prior to exhumation (Figures 3a and 3b). The maximum burial depth of exhumed UHP rocks increases toward the south. A stress switch from compression to extension occurs as a result of upper-plate rotation since 8 Myr, which creates a conduit that allows buoyancy-driven exhumation of previously subducted continental-margin rocks. All our models produced exhumation without slab breakoff (Figures 3c–3e). The southern stretch of the subduction wedge experiences a higher exhumation rate of ∼30 mm/yr during 8–13 Myr compared to the northern stretch, because of the southward increase in divergence (35 vs. 60 km) caused by counterclockwise rotation of the upper plate. These differential exhumation rates cause deeply buried crust to rise to the surface more quickly within the subduction conduit of the southern orogen. Additionally, the underlying mantle-wedge rocks undergo exhumation synchronously with UHP rocks, filling the relatively shallow levels of the subduction conduit. The southward increase in divergence further results in the mantle wedge being ultimately emplaced at shallow depths beneath the southern UHP metamorphic dome.

The *P-T-t* paths of some of the highlighting tracers in our models offer a more explicit illustration of the three stages of continental-margin crust evolution along the trench: subduction, stagnation, and exhumation (Figure 4). Pressure and temperature rise nearly linearly during a prograde deep subduction stage, causing UHP rock

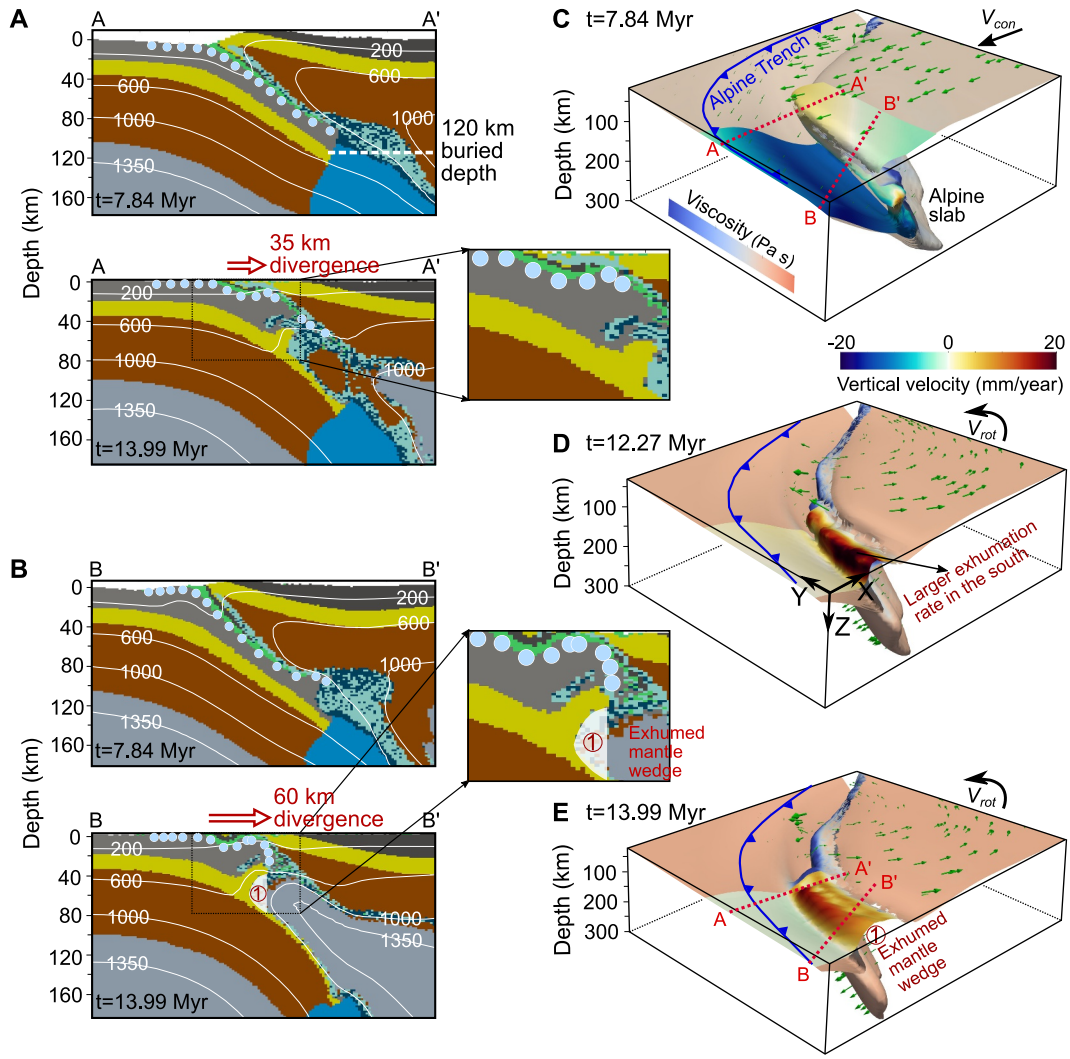

Figure 3. Model results showing the dynamics of the subduction and exhumation of continental-margin crust. (a, b) The material phases of two vertical profiles (AA′ and BB′) in the Reference model. The locations of these two profiles are shown in panels (c, e). Isotherms (in °C) are indicated by white lines. The red number 1 that is located in the white shade represents the exhumed mantle wedge beneath the southern metamorphic dome in panel (b). Colors and legends are described in Figure 2. (c–e) 3-D perspective views of the velocity and viscosity fields in the Reference model. The blue sawtooth curves represent the trench positions, while the plate flow directions are represented by the green and black arrows.

metamorphism in the continental-margin crust. The peak pressure for these tracers is reached at different computed times, and it may be inferred that not all of the buried rocks enter the stagnation stage simultaneously. At this stage, some tracers from UHP metamorphic rocks even experience almost isobaric heating. They then experienced a large and nearly isothermal pressure drop, which indicated rapid exhumation. Since approaching closer to the Earth surface, these tracers of UHP rocks enter a slower exhumation stage due to a decrease in the density contrast with surrounding rocks. The metamorphic peaks of UHP rocks in the model increase southward, but they are within the coesite-stability field even in the north. This is in line with geological observations showing maximum temperature and pressure in the southern Dora-Maira (~780°C and ~3.2 GPa; Rubatto & Hermann, 2001), and the presence of coesite at various locations throughout the Eocene eclogite belt.

4.2. Varied Model Setups With Adria Rotation Rate

Variations in the counterclockwise rotation rates (V_{rot}) of the upper-plate Adria do not change the subduction-stagnation-exhumation evolution style of exhumed UHP rocks, but alter their metamorphic peaks or the

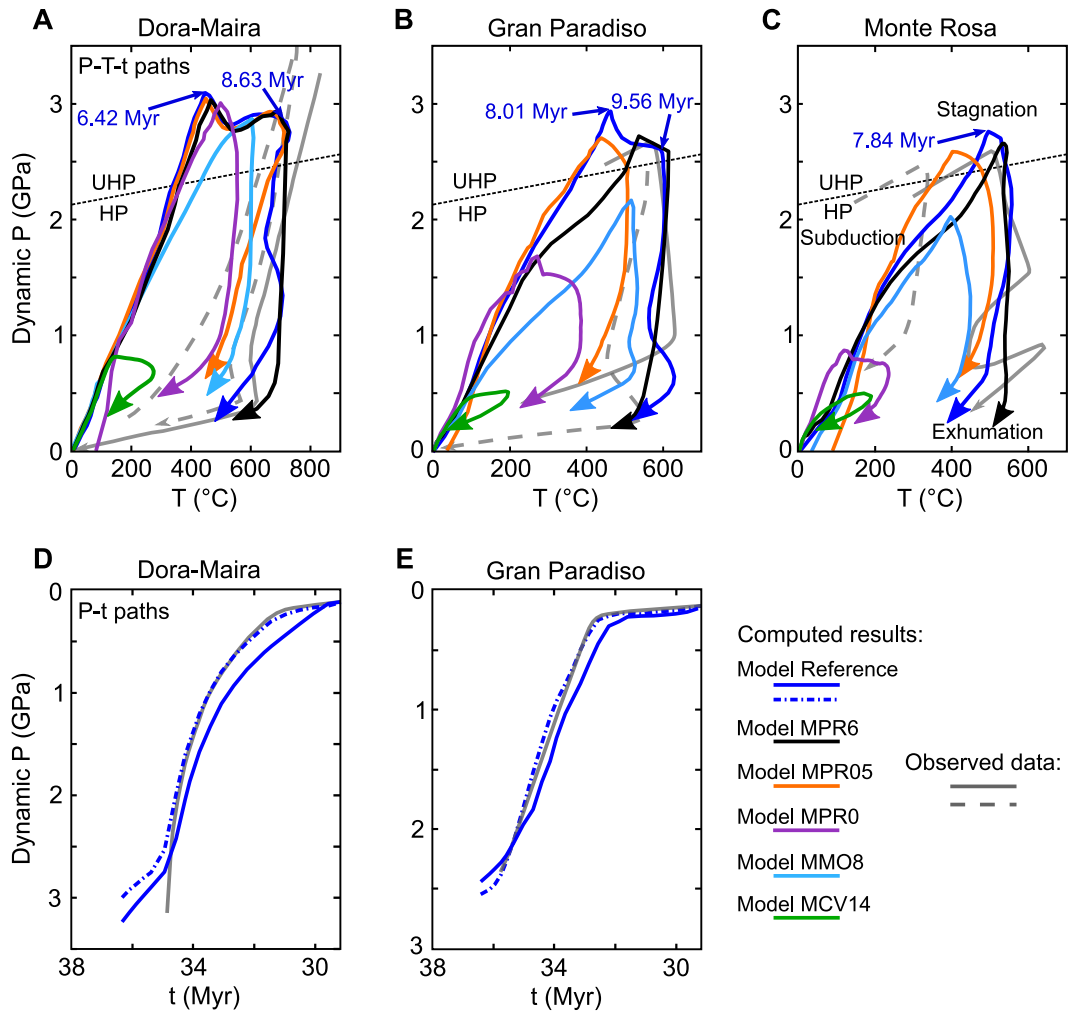

Figure 4. Dynamic pressure-temperature-time and pressure-time paths for several tracers in the calculated models, with comparison to observational data. (a-c) *P-T-t* paths in three different regions of the Western Alps orogen from south to north. The gray curves indicate observations that are the same as Figure 1b, while the other lines represent our computed results. (d-e) *P-t* paths in the Dora-Maira and Gran Paradiso domes of this orogen. The blue curves represent the calculated results from the Reference model, and the gray curves indicate observations from Malusà et al. (2011) and references therein.

mantle wedge exhumation. A fast counterclockwise rotation, such as 6°/Myr in the MPR6 model, results in the UHP rock metamorphic peaks to increase southward along the orogen strike, which is similar to the Reference model (Figure 4). Although this fast rotation causes an increased exhumation rate in the south of the orogen, the mantle wedge remains exhumed beneath the southern dome, where the amount of divergence is ~60 km (Figure 5a). Furthermore, when the rotation rate is decreased to 0.5°/Myr in the MPR05 model, the exhumation rate of UHP rocks is significantly lower throughout the whole orogen (Figure 5b). The Monte Rosa dome of the northern Western Alps has a lower pressure peak as a result of this lowering (Figure 4). Notably, UHP metamorphic pressure is absent in the Gran Paradiso and Monte Rosa domes of the MPR0 model, which excludes the Adria rotation setting.

Additional variables, such as the Moho temperature for the Adriatic microcontinent (T_{moho}) and the plate convergence time, have been determined for a more accurate simulation of the exhumation process. Model results indicate that the differential exposure of HP-UHP metamorphic rocks occurs for distinct T_{moho} values on the Adriatic microcontinent. Similar to the Reference model, the MMO8 model with an elevated T_{moho} of 800°C achieved the highest metamorphic peak in the Dora-Maira, identifying three evolution stages in the orogenic belt (Figure 4). However, the elevated T_{moho} causes severe deformation that forms zones of strain localization in the overriding Adriatic microcontinent during convergence, which differs from the Reference

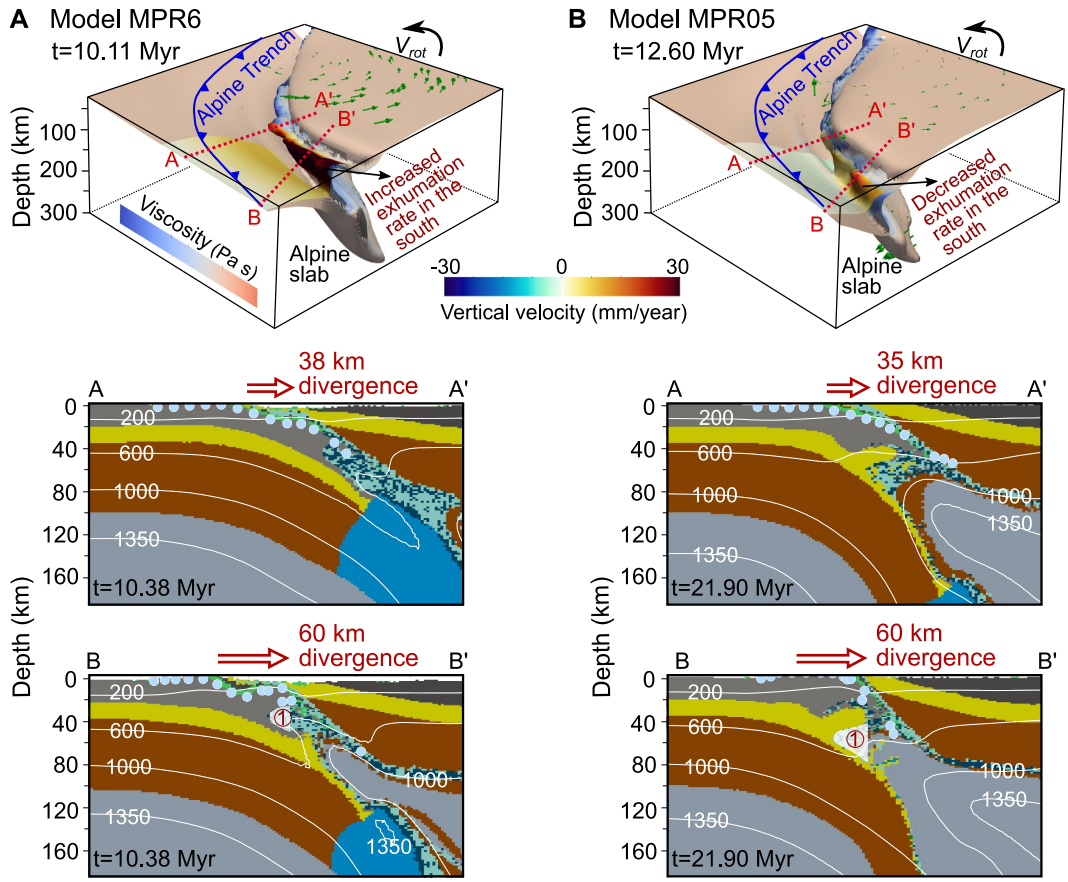

Figure 5. Effects of (a) fast counterclockwise rotation of 6°/Myr in the MPR6 model and (b) slow counterclockwise rotation of 0.5°/Myr in the MPR05 model on model results. Each section includes 3-D perspective views of the velocity and viscosity fields in the first row and two vertical profiles (AA′ and BB′) in the second and third rows. The blue sawtooth curves and green arrows are illustrated in Figure 3c. Colors and legends are described in Figure 2, while the red number 1 and isotherms are illustrated in Figure 3b.

model (Figures 6a and 6b). Due to this, crustal deep subduction is inhibited, lowering the buried depth of the European continental-margin crust, even to ~80 km in the northern orogen (Figure 6c). While the peak pressure and mantle wedge exumation in the Dora-Maira dome remain unchanged, the peak pressures in the Monte Rosa and Gran Paradiso domes decrease to a HP degree (Figure 4). Only HP metamorphic rocks are exposed throughout the orogenic belt during 14 Myr of continuous convergence in the MCV14 model, indicating that UHP exhumation driven by continuous westward motion (Handy et al., 2010) is not feasible.

4.3. Model Evolution Incorporating an Abrupt Change in Adria Motion

In scenario (ii), we consider an abrupt change in Adria motion, without rotation, starting at 8 Myr. Models MPD30 (northeastward divergent motion at 30 mm/yr) and MDC180 (eastward divergent motion at 15 mm/yr) result in different amounts of upper-plate divergent motion (Figures 7a and 7b), although both produce *P-T-t* paths that are similar to those of the Reference model (Figure 8). Moreover, UHP conditions are maintained in the MPD60 model with a fast northeastward divergence of 60 mm/yr. When the northeastward divergence rate (V_{div}) drops to 10 mm/yr in the MPD10 model and Adria motion changes from west to north in the MDC90 model, the peak pressure and temperature in the northern region (Monte Rosa) are reduced, potentially reaching HP metamorphic conditions (Figure 8).

Calculations were performed to test the combined effects of Adria counterclockwise rotation and divergent motion northwestward. Our results show that the differential exhumation of HP-UHP rocks is essentially unrelated to the imposed sequence and duration time of these two parameters (Table 3). When the Adria

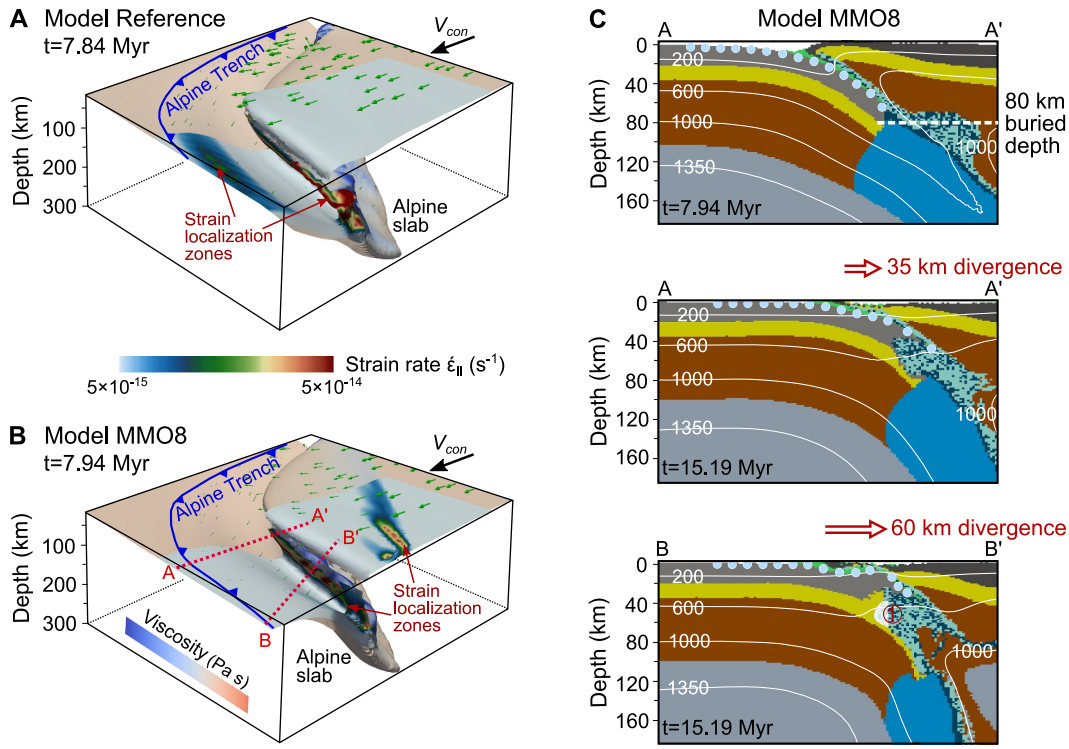

Figure 6. Effects of upper-plate Moho temperature on model results. 3-D perspective views of the velocity and strain rate fields in panel (a) the Reference model with Moho temperature of 600°C and (b) the MMO8 model with Moho temperature of 800°C.

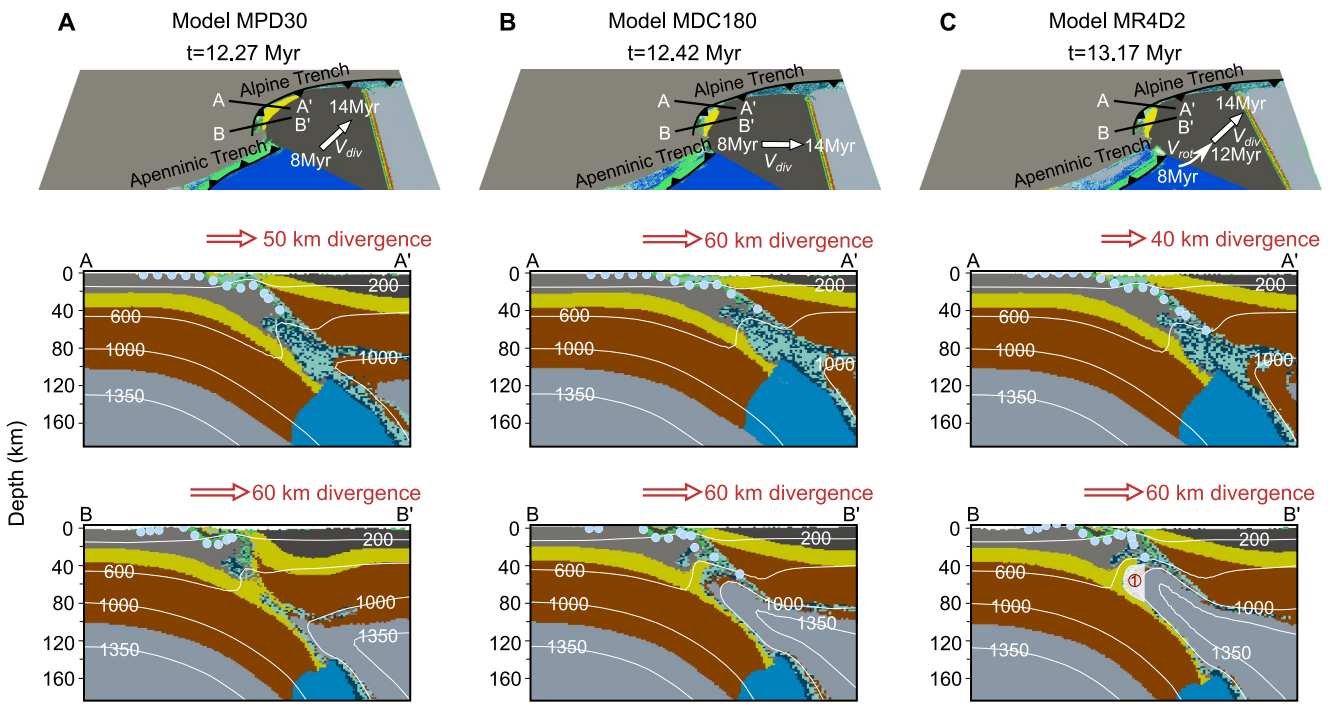

Figure 7. Effects of Adria divergence without rotation on model results. The material phases are shown in panel (a) the MPD30 model with motion change from westward to northeastward at 8 Myr, (b) the MDC180 model with motion change from westward to eastward at 8 Myr, and (c) the MR4D2 model with counterclockwise rotation at 8 Myr followed by a sudden shift to the northeast at 12 Myr. Each section includes top views in the first row and two vertical profiles (AA′ and BB′) in the second and third rows.

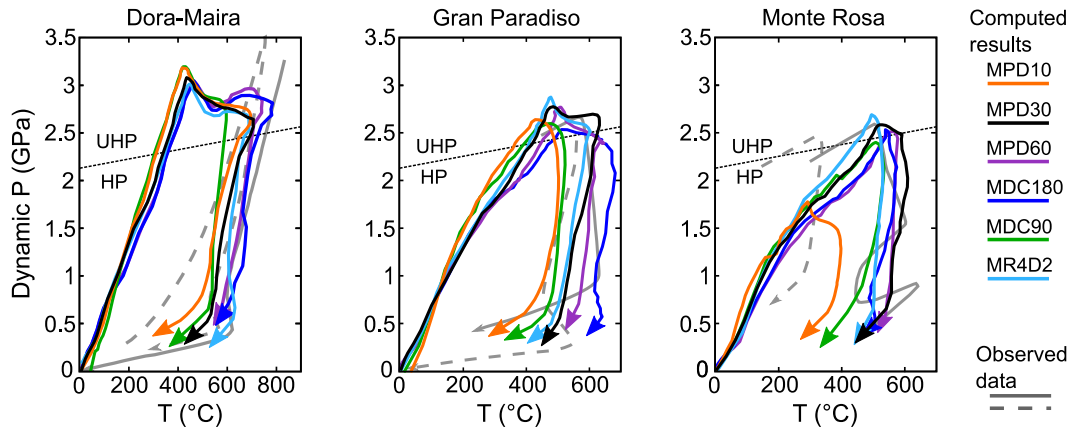

Figure 8. Dynamic pressure-temperature-time paths in three different regions of the Western Alps from south to north for several tracers in the calculated models, with comparison to observational data. The gray curves indicate observations that are the same as Figure 1b, while the other lines represent our computed results.

counterclockwise rotation serves as the main driver of exhumation, incorporating both rotation and divergence, it can provide comparable outcomes with the Reference model. Model MR4D2, which features 4 Myr of counterclockwise rotation followed by 2 Myr of divergence northwestward from the trench, results in divergences of ∼40–∼60 km from north to south (Figure 7c). An exhumed mantle wedge also occurs beneath the southern Western Alps (Dora-Maira dome) in the MR4D2 model. These findings are further corroborated by additional simulations that adopt various combinations of rotation and divergence: models MR2D4 (2 Myr of rotation followed by 4 Myr of divergence), MD2R4 (2 Myr of divergence followed by 4 Myr of rotation), and MD4R2 (4 Myr of divergence followed by 2 Myr of rotation), with full parameter specifications provided in Table 3.

5. Discussion

5.1. Role of Upper-Plate Adria Counterclockwise Rotation

The channel flow, which is composed of the opposing influences of the Couette and Poiseuille flows, regulates the persistence and transition of subduction and exhumation in 2-D space profile (Figure S2 in Supporting Information S1; Erdman & Lee, 2014; Guillot et al., 2001; Horodyskyj et al., 2009; Raimbourg et al., 2007). It can be simplified by

$$V_{\text{channel}}(x,y) \approx \frac{\Delta\rho_{\text{channel}}\, g\, \sin\theta\, h^2}{\eta},$$

where $\Delta\rho_{\text{channel}}$ is the density contrast of the densities of surrounding mantle and rocks in subduction channel, h the channel thickness, θ the subduction angle, and η the assumed uniform viscosity (see the detailed analytic procedure in our earlier work by Wang et al. (2021)). The down-channel Couette flow dominates the crustal flow of the continental margin during the subduction stage, which is driven by the external pushing force and slab pull. It is progressively reduced due to the weakening subduction channel caused by heating from overriding thermal Adria, which is a thermal weakening mechanism (e.g., Burov et al., 2014; Wang et al., 2021). Prior to upper-plate Adria counterclockwise rotation at 8 Myr, the crustal flow at the upper surface of the subduction channel even stagnates and reverses (Figures 4a–4c). Once regional extension initiates, residual continental-margin crustal materials travel upward and exhibit up-channel Poiseuille flow due to h and $\Delta\rho_{\text{channel}}$ increase and η decreases. Despite this overall upward movement, the upper-plate lithosphere acts as a physical barrier during the initial exhumation stage, inhibiting the upward migration of specific tracers derived from UHP metamorphic rocks (Figure S2 in Supporting Information S1). This barrier effect induces nearly isobaric heating followed by isothermal decompression. In the Dora-Maira dome of the Reference model, for example, peak pressure occurs at 6.42 Myr (Figure 4a); peak temperature subsequently rises isobarically between 6.42 and 8.63 Myr, after which the system undergoes isothermal decompression.

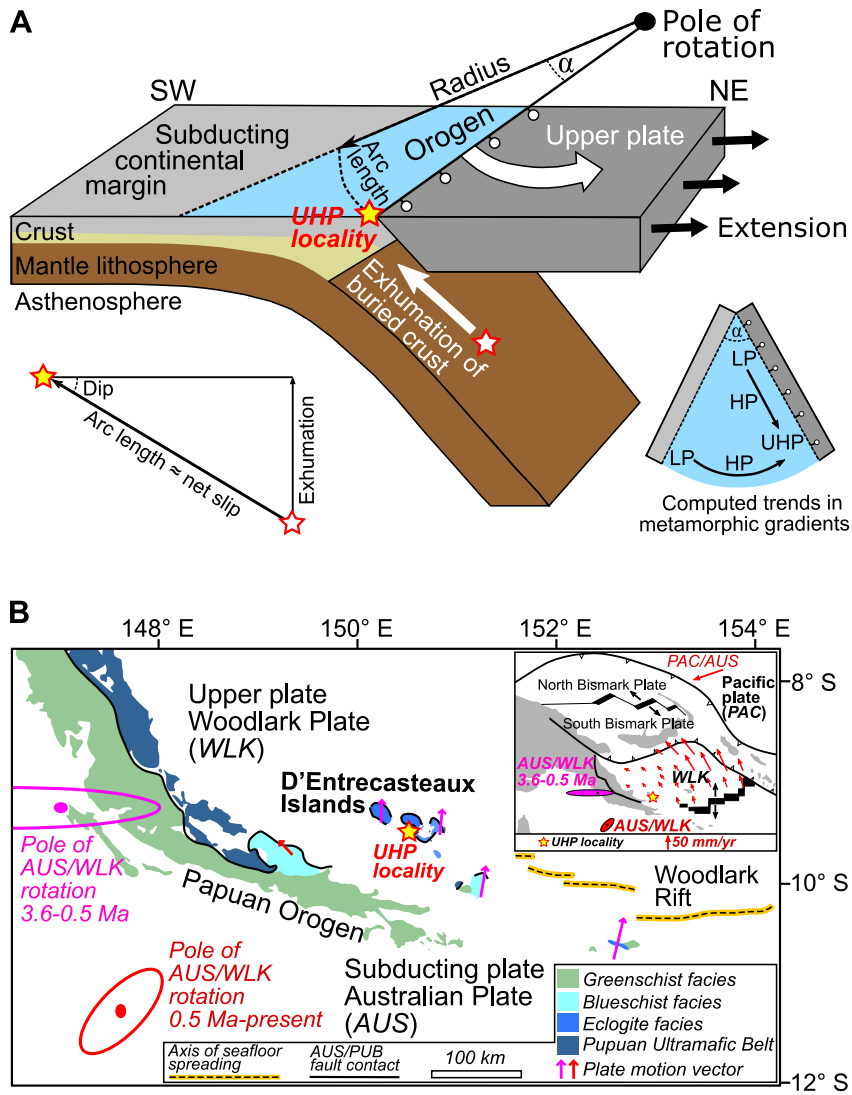

Figure 9. (a) Schematic diagram showing UHP rock exhumation induced by upper-plate counterclockwise rotation (Webb et al., 2008). The white and yellow stars bracked by red lines represent the pre- and post-exhumation positions of UHP metamorphic rocks. A pie-slice diagram for plan views of the exhumed HP-UHP rocks is inserted on the bottom right, where arrows indicate the predicted trends in peak metamorphic gradients (acronyms: LP, lower pressure; HP, high pressure; UHP, ultrahigh pressure). (b) Simplified tectonic map of south-eastern Papua New Guinea, with the eastern part inserted on the top right (Wallace et al., 2014; Webb et al., 2008). Pink and red error ellipses represent poles of rotation for 3.6–0.5 Ma (Taylor et al., 1999) and the present (Wallace et al., 2004), respectively. Acronyms: AUS, Australian Plate; PAC, Pacific Plate; PUB, Papuan Ultramafic Belt; WLK, Woodlark Plate.

Upper-plate counterclockwise rotation can cause different divergence between the upper plate and the trench in the orogen, making the channel flow in our 3-D geodynamic models even more complicated. The amount of divergent motion (arc length) is determined based on the distance from the pole of rotation in the Adria adjacent to the Alpine trench (radius) and the rotation angle (α; Figure 9a). With a rotation angle of ~12° in the Reference model (Table 3), the resulting divergence is ~60 km in the southern Western Alps (BB′) far away from the pole, whereas being ~35 km in the northern Western Alps (AA′) close to the pole (Figure 3). This is consistent with previous geodynamic reconstructions of the Adria-Europe plate-boundary zone (Malusà et al., 2015; Solarino et al., 2018) and 2-D exhumation models (e.g., Liao et al., 2018). The southward increase in divergence along the orogen strike yields a greater thickness h of the subduction channel in the south than in the north during regional extension (Figure S2 in Supporting Information S1). This thicker channel, coupled with elevated temperatures that drive a reduction in viscosity η, further promotes Poiseuille flow and thus leads to accelerated exhumation in

the southern segment of the subduction wedge (Figure 3). Even with variations in the upper-plate rotation rate and Moho temperature, the southward increase in divergence remains consistent during upper-plate counterclockwise rotation (Figures 5 and 6). In contrast, this southward divergence signal becomes undetectable once the Adria undergoes abrupt kinematic changes without concurrent rotation (Figures 7a and 7b). Additionally, the mantle wedge and UHP metamorphic rocks in the Western Alps undergo differential exhumation in response to this southward increasing divergence. Collectively, these effects give rise to a scenario where the peak pressure and temperature conditions of individual tracers are achieved at distinct computational timesteps, indicating the diversity of *P-T-t* evolution (Li, 2014; Sizova et al., 2024).

5.2. Differential Exhumation of the Western Alps Mantle Wedge

According to our models, the subduction wedge in the Western Alps experiences a southward increase in exhumation rate due to the counterclockwise rotation of the Adriatic upper plate (Figures 3 and 5). In the southern orogen, the peak exhumation rate is higher (∼30 mm/yr) during the isothermal decompression stage and then significantly decreases, which accords with the observed data (Malusà et al., 2011). These processes of evolution from our models correspond to the deposition of sediments on top of the southern portion of the Eclogite belt (Federico et al., 2005; Malusà & Garzanti, 2012). As shown in Figure 3, the mantle wedge exhumes in the south due to the larger exhumation rate than in the north. Recent seismic experiments in the Western Alps (Malusà et al., 2021; Solarino et al., 2024) propose that a prominent high velocity body (Vp of ∼7–7.5 km/s) indicates the presence of the exhumed mantle-wedge beneath the Dora-Maira UHP dome (BB′ profile in Figure 1a). Beneath the Gran Paradiso UHP dome, however, no high-Vp body reflecting an exhumed mantle wedge is observed (AA′ profile in Figure 1a). Therefore, by comparing first-order features at depth at the similar vertical profiles, our 3-D model predictions of the differential exhumation of the mantle wedge replicate these geologic observations.

5.3. Differential Exhumation of UHP Metamorphic Rocks in the Western Alps

2-D exhumation models driven by upper-plate divergent motion (e.g., Liao et al., 2018) have successfully reproduced the differential exhumation in the direction perpendicular to the orogen strike, as obtained by observations (e.g., Malusà et al., 2011, 2015) and our 3-D models. The crustal materials of the continental margin close to the upper plate experience prolonged subduction and reach a higher metamorphic peak pressure (Figure 9a). UHP metamorphic rocks are thus exposed in the east, as indicated by the red dashed curve in Figure 1a (see detailed calculations in Text S1 in Supporting Information S1; Yamato & Brun, 2017), whereas solely HP rocks are only displayed in the west, as depicted by the blue dashed curve Figure 1a. However, 2-D models were unable to test the differential sampling depth of exhumed UHP rocks along the orogen strike. In the Western Alps, the metamorphic peaks tend to increase southward (Groppo et al., 2019; Luisier et al., 2019; Rubatto & Hermann, 2001), although each metamorphic terrane exhibits a wide range of peak conditions. For instance, a UHP peak pressure at 3.5 GPa is observed in the Dora-Maira dome (Rubatto & Hermann, 2001), while a lower UHP peak pressure is recorded at 2.4 GPa in the Monte Rosa dome (Le Bayon et al., 2006). The diverse *P-T-t* and *P-t* paths (Figures 4 and 8) of the European continental-margin crustal materials in our simulations reveal the complex HP-UHP exposure processes occurring within the orogenic belt. We find that upper-plate counterclockwise rotation induces the rapid exhumation of UHP rocks from different subduction depths in three UHP domes of the Western Alps, alongside the differential exhumation of the mantle wedge. Modeled peak conditions in our simulations exhibit increasing trends toward the south due to an arcuate Alpine trench setting that lowers the convergence rate and down-channel Couette flow in that direction, with their range aligning well with observed data (Malusà et al., 2011; Radulescu et al., 2009; Rubatto & Hermann, 2001).

Previous studies mostly focus on two independent mechanisms driving the differential exhumation of UHP rocks, including subducted microplate rotation (Bottrill et al., 2014; Burov et al., 2014; Hacker & Gerya, 2013; Webb et al., 2008; Zhang & Wang, 2020) and lithological heterogeneity of the continental margin crust (e.g., Ganade et al., 2024). According to 3-D numerical modeling (Bottrill et al., 2014), diachronous collisions cause the subducted continent to rotate and reverse, only causing exhumation at the initial collision site. In this study, we find that upper-plate rotation can also induce the subducted continental-margin crust to exhume from different subduction depths throughout the orogenic belt (Figure 9a). Based on the replicated first-order characteristics in the Western Alps, including divergent motion, exhumed mantle wedge, and UHP metamorphic rocks, the upper-plate counterclockwise model proves to be more robust in present 3-D double subduction systems. Furthermore, 2-D numerical models (Ganade et al., 2024) suggest that magma-poor and magma-rich rifted margins cause

distinct exhumation magnitudes, indicating that strike-parallel lithological heterogeneity of continental margin crust may affact 3-D UHP differential exhumation. The evolution of the Western Alps starts from an asymmetric magma-poor rifted margin, but lateral variations exist on the European side likely inherited from the Variscan orogeny. If hypothetically the magma-poor southern segment was set in correspondence with a portion of Variscan crust characterized by weaker siliciclastic rocks, this could act as an additional synergistic factor to amplify the along-strike differential exhumation captured by our 3-D numerical models with a homogeneous continental-margin crust for simplicity.

5.4. Differential Exhumation of Other UHP Terranes

Lateral variations in pressure peak conditions reported from other UHP terranes worldwide (e.g., Wang et al., 2003; Webb et al., 2008) may be linked to variable divergence rates during upper-plate rotation. For example, the Australian and Pacific Plates converge obliquely at 100–110 mm/yr in the present-day tectonic setting of Papua New Guinea, which is later fragmented into several microplates (Figure 9b). One of these microplates, the Woodlark Plate, causes the Woodlark Rift to shift from convergence to extension by rotating counterclockwise with respect to the Australian Plate along a nearby pole of rotation for 3.6–0.5 Ma and the present (pink and red error ellipses in Figure 9b; Taylor et al., 1999; Wallace et al., 2004, 2014; Webb et al., 2008). The amounts of upper-plate divergent motion increase eastward along-strike in the Woodlark Basin due to the greater distance from the pole of rotation in that direction (Petersen & Buck, 2015). These result in the exhumation of the previously buried rocks of the Australian continental margin via the normal-sense reactivation of the former subduction thrust. The peak metamorphic gradients of exhumed UHP rocks are predicted to rise in the direction of upper-plate rotation and increase divergence along the orogen strike (Webb et al., 2008), which aligns with our simulated results (the bottom right insert in Figure 9a). Such change trends are emergent in the westward younging metamorphism of the eclogite facies, which are exposed near the Australian–Woodlark Plate boundary in the D'Entrecasteaux Islands (e.g., Baldwin et al., 2006; Monteleone et al., 2007).

Additionally, the Dabie Shan UHP terrane, which was formed in the Triassic by subduction of the Yangtze Craton beneath the North China Craton, exhibits an eastward and northward rise in peak metamorphism (e.g., Hacker et al., 1998, 2004; Liou et al., 1996, 2009). This former rise is due to the eastward increasing amounts of extension farther from the pole of rotation, as predicted by Guo et al. (2012) and our simulated results (Figure 9a). Similar to the southern Western Alps, the seismic velocity signature of Moho-type interfaces linked to an exhumed mantle wedge beneath the exhumed UHP rocks of the South and Central Dabie is also revealed (Luo et al., 2012; Solarino et al., 2024). Similarly, UHP rock exhumation in the Himalaya Tso Morari complex is thought to be linked to a significant rotation of the India-Eurasia-Australia plate network at ∼50–46 Ma (Bidgood et al., 2024). Therefore, our model demonstrates that increased plate divergence due to upper-plate rotations not only explain lateral variations in the deep structure of the fossil continental subduction zone, but may also explain the lateral variation in pressure peaks observed in many UHP terranes where the kinematics are no longer ascertainable.

5.5. Model Limitations

This is the first 3-D geodynamic model to investigate the potential differential exhumation of UHP and mantle-wedge rocks driven by increasing plate divergence in the Western Alps. Model parameters have been deliberately simplified, given the complexity of natural subduction interfaces. These interfaces are influenced not only by temperature (e.g.,Turino & Holt, 2024) incorporated in this study, but also by fluid release and serpentinization (e.g., Gerya et al., 2008) omitted here. Fluids released by dehydration reactions at the interface of the Tethys oceanic slab, alongside mantle-wedge serpentinization, may facilitate exhumation of UHP rocks by weakening the subduction channel (e.g., Liao et al., 2018). Nevertheless, our results demonstrate that even with simplified parameterization, our models successfully reproduce key characteristics of both shallow and deep structures that match observations from the Western Alps.

6. Conclusions

In conclusion, we present 3-D geodynamic models to investigate the differential exposure of UHP metamorphic rocks in two adjacent subduction systems that dip oppositely and apply them to the metamorphic terranes in the Western Alps. In systematic simulations, we test two end-member scenarios of upper-plate motion, that is, divergent motion away from the trench and Adria counterclockwise rotation with variation in the plate

convergence time and Moho temperature for the Adriatic microcontinent. The simulations are characterized in terms of divergent motion, exhumed mantle wedge, and exhumed HP-UHP rocks in the orogen, which are compared with constraints from the Western Alps. The following conclusions can be reached based on our model results.

1. Following the Tethys oceanic slab, the continental margin experiences deep subduction along the Alpine trench during plate convergence in our 3-D models. It is deeply buried to the eclogite peak in the orogen promoted by the low Moho temperature for the upper-plate Adria. The maximum burial depth increases toward the south due to an arcuate Alpine trench configuration that lowers the convergence rate and down-channel Couette flow in that direction.
2. Both end-member scenarios of upper-plate motion can successfully reproduce the pressure-temperature-time paths observed in exhumed UHP rocks by shifting the regional tectonics from compression to extension. The UHP metamorphic peak, which is influenced by the rate and direction of divergent motion without rotation, exhibits a unidirectional southward increase along the orogen strike.
3. Only in the simulations where the counterclockwise rotation of the upper plate acts as the primary driver of exhumation do the resulting characteristics of the surface and deep structure fit with those observed in the Western Alps. They include the southward-increasing amounts of upper-plate divergence away from the Alpine trench, which induces the presence of an exhumed mantle wedge beneath the southern UHP domes and its absence beneath the northern UHP domes.
4. Finally, model results may be exported to other subduction zones where kinematic constraints suggest a component of upper-plate rotation, such as eastern Papua New Guinea, and to older subduction zones where the kinematics is poorly assessed.

Conflict of Interest

The authors declare no conflicts of interest relevant to this study.

Data Availability Statement

Numerical models in this study were conducted with the open-source finite difference code LaMEM, which is available at Zenodo (https://zenodo.org/records/15524303; Popov & Kaus, 2025). The data (Figures 3 and 5–7) are available at figshare (Wang, 2025).

Acknowledgments
This work was supported by the National Key R&D Program of China (Grant 2024YFF0807400), and the National Natural Science Foundation of China (Grants 92355301, 42488201). We would like to thank Jianfeng Yang for the constructive discussions on the model results. We also thank Editor David Hernández Uribe for editorial handling and reviewer Carlos E. Ganade and Valeria Turino for their accurate and constructive reviews that improved the original manuscript.

References

Agard, P. (2021). Subduction of oceanic lithosphere in the Alps: Selective and archetypal from (slow-spreading) oceans. *Earth-Science Reviews*, *214*(January), 103517. https://doi.org/10.1016/j.earscirev.2021.103517

Baldwin, S. L., Webb, L. E., Monteleone, B., Little, T. A., Fitzgerald, P. G., Peters, K., & Chappell, J. L. (2006). Continental crust subduction and exhumation: Insights from eastern Papua New Guinea. *Geochimica et Cosmochimica Acta*, *70*(Supplement), A31. https://doi.org/10.1016/j.gca.2006.06.171

Bidgood, A. K., Parsons, A. J., Roberts, N. M. W., Waters, D., Tapster, S., & Gopon, P. (2024). The geodynamic significance of continental UHP exhumation: New constraints from the Tso Morari Complex, NW Himalaya. *Tectonics*, *43*(5), e2023TC007976. https://doi.org/10.1029/2023tc007976

Bottrill, A. D., Van Hunen, J., Cuthbert, S. J., Brueckner, H. K., & Allen, M. B. (2014). Plate rotation during continental collision and its relationship with the exhumation of UHP metamorphic terranes: Application to the Norwegian caledonides. *Geochemistry, Geophysics, Geosystems*, *15*(5), 1766–1782. https://doi.org/10.1002/2014GC005253

Brun, J., & Faccenna, C. (2008). Exhumation of high-pressure rocks driven by slab rollback. *Earth and Planetary Science Letters*, *272*(1–2), 1–7. https://doi.org/10.1016/j.epsl.2008.02.038

Burov, E., Francois, T., Agard, P., Le Pourhiet, L., Meyer, B., Tirel, C., et al. (2014). Rheological and geodynamic controls on the mechanisms of subduction and HP/UHP exhumation of crustal rocks during continental collision: Insights from numerical models. *Tectonophysics*, *631*(C), 212–250. https://doi.org/10.1016/j.tecto.2014.04.033

Butler, J. P., Beaumont, C., & Jamieson, R. A. (2013). The Alps 1: A working geodynamic model for burial and exhumation of (ultra)high-pressure rocks in alpine-type orogens. *Earth and Planetary Science Letters*, *377–378*, 114–131. https://doi.org/10.1016/j.epsl.2013.06.039

Chopin, C. (1984). Coesite and pure pyrope in high grade blueschists of the Western Alps: A first record and some consequences. *Contributions to Mineralogy and Petrology*, *86*(2), 107–118. https://doi.org/10.1007/bf00381838

Crameri, F., Schmeling, H., Golabek, G. J., Duretz, T., Orendt, R., Buiter, S. J. H., et al. (2012). A comparison of numerical surface topography calculations in geodynamic modelling: An evaluation of the "sticky air" method. *Geophysical Journal International*, *189*(1), 38–54. https://doi.org/10.1111/j.1365-246x.2012.05388.x

Davies, J. H., & von Blanckenburg, F. (1995). Slab breakoff: A model of lithosphere detachment and its test in the magmatism and deformation of collisional orogens. *Earth and Planetary Science Letters*, *129*(1–4), 85–102. https://doi.org/10.1016/0012-821X(94)00237-S

Dewey, J. F., Helman, M. L., Knott, S. D., Turco, E., & Hutton, D. H. W. (1989). Kinematics of the western mediterranean. *Geological Society, London, Special Publications*, *45*(1), 265–283. https://doi.org/10.1144/GSL.SP.1989.045.01.15

Dumont, T., Schwartz, S., Guillot, S., Malusà, M., Jouvent, M., Monié, P., & Verly, A. (2022). Cross-propagation of the western Alpine orogen from early to late deformation stages: Evidence from the Internal Zones and implications for restoration. *Earth-Science Reviews*, *232*, 104106. https://doi.org/10.1016/j.earscirev.2022.104106

Duretz, T., & Gerya, T. V. (2013). Slab detachment during continental collision: Influence of crustal rheology and interaction with lithospheric delamination. *Tectonophysics*, *602*, 124–140. https://doi.org/10.1016/j.tecto.2012.12.024

Erdman, M. E., & Lee, C. T. A. (2014). Oceanic- and continental-type metamorphic terranes: Occurrence and exhumation mechanisms. *Earth-Science Reviews*, *139*, 33–46. https://doi.org/10.1016/j.earscirev.2014.08.012

Faccenna, C., Becker, T. W., Auer, L., Billi, A., Boschi, L., Brun, J. P., et al. (2014). Mantle dynamics in the Mediterranean. *Reviews of Geophysics*, *52*(3), 283–332. https://doi.org/10.1002/2013RG000444

Federico, L., Capponi, G., Crispini, L., Scambelluri, M., & Villa, I. M. (2005). 40Ar/39Ar dating of high-pressure rocks from the Ligurian Alps: Evidence for a continuous subduction–exhumation cycle. *Earth and Planetary Science Letters*, *240*(3–4), 668–680. https://doi.org/10.1016/j.epsl.2005.09.062

Ganade, C. E., Riel, N., Manatschal, G., Tesser, L. R., Hermann, J., Rubatto, D., et al. (2024). Exhumation of ultra-high pressure (UHP) rocks modulated by rifted margin-subduction feedback: Implications for their preservation in old collisional orogens. *Earth and Planetary Science Letters*, *643*, 118893. https://doi.org/10.1016/j.epsl.2024.118893

Gasco, I., Borghi, A., & Gattiglio, M. (2010). Metamorphic evolution of the Gran Paradiso Massif: A case study of an eclogitic metagabbro and a polymetamorphic glaucophane-garnet micaschist. *Lithos*, *115*(1–4), 101–120. https://doi.org/10.1016/j.lithos.2009.11.009

Gasco, I., Borghi, A., & Gattiglio, M. (2011). P-T Alpine metamorphic evolution of the Monte Rosa nappe along the Piedmont Zone boundary (Gressoney Valley, NW Italy). *Lithos*, *127*(1–2), 336–353. https://doi.org/10.1016/j.lithos.2011.09.007

Gerya, T. V., Perchuk, L. L., & Burg, J. P. (2008). Transient hot channels: Perpetrating and regurgitating ultrahigh-pressure, high temperature crust–mantle associations in collision belts. *Lithos*, *103*(1–2), 236–256. https://doi.org/10.1016/j.lithos.2007.09.017

Ghignone, S., Gilio, M., Borghini, A., Boero, F., Bruno, M., & Scaramuzzo, E. (2024). Mineralogical and petrological constraints and tectonic implications of a new coesite-bearing unit from the Alpine Tethys oceanic slab (Susa Valley, Western Alps). *Lithos*, *472*, 107575. https://doi.org/10.1016/j.lithos.2024.107575

Ghignone, S., Scaramuzzo, E., Bruno, M., & Livio, F. A. (2023). A new UHP unit in the Western Alps: First occurrence of coesite from the Monviso Massif (Italy). *American Mineralogist*, *108*(7), 1368–1375. https://doi.org/10.2138/am-2022-8621

Groppo, C., Ferrando, S., Gilio, M., Botta, S., Nosenzo, F., Balestro, G., et al. (2019). What's in the sandwich? New P–T constraints for the (U)HP nappe stack of southern Dora-Maira Massif (Western Alps). *European Journal of Mineralogy*, *31*(4), 665–683. https://doi.org/10.1127/ejm/2019/0031-2860

Guillot, S., Hattori, K., Agard, P., Schwartz, S., & Vidal, O. (2009). Exhumation processes in oceanic and continental subduction contexts: A review. In *Subduction zone geodynamics* (pp. 175–205). Springer. https://doi.org/10.1007/978-3-540-87974-9_10

Guillot, S., Hattori, K. H., De Sigoyer, J., Nägler, T., & Auzende, A. L. (2001). Evidence of hydration of the mantle wedge and its role in the exhumation of eclogites. *Earth and Planetary Science Letters*, *193*(1–2), 115–127. https://doi.org/10.1016/S0012-821X(01)00490-3

Guo, X., Encarnacion, J., Xu, X., Deino, A., Li, Z., & Tian, X. (2012). Collision and rotation of the South China block and their role in the formation and exhumation of ultrahigh pressure rocks in the Dabie Shan orogen. *Terra Nova*, *24*(5), 339–350. https://doi.org/10.1111/j.1365-3121.2012.01072.x

Hacker, B. R., & Gerya, T. V. (2013). Paradigms, new and old, for ultrahigh-pressure tectonism. *Tectonophysics*, *603*, 79–88. https://doi.org/10.1016/j.tecto.2013.05.026

Hacker, B. R., Ratschbacher, L., & Liou, J. G. (2004). Subduction, collision and exhumation in the ultrahigh-pressure Qinling-Dabie orogen. *Geological Society, London, Special Publication*, *226*(1), 157–175. https://doi.org/10.1144/gsl.sp.2004.226.01.09

Hacker, B. R., Ratschbacher, L., Webb, L., Ireland, T., Walker, D., & Shuwen, D. (1998). U/Pb zircon ages constrain the architecture of the ultrahigh-pressure Qinling-Dabie Shan Orogen, China. *Earth and Planetary Science Letters*, *161*(1–4), 215–230. https://doi.org/10.1016/s0012-821x(98)00152-6

Handy, M. R., M. Schmid, S., Bousquet, R., Kissling, E., & Bernoulli, D. (2010). Reconciling plate-tectonic reconstructions of Alpine Tethys with the geological-geophysical record of spreading and subduction in the Alps. *Earth-Science Reviews*, *102*(3–4), 121–158. https://doi.org/10.1016/j.earscirev.2010.06.002

Hirth, G., & Kohlstedt, D. (2004). Rheology of the upper mantle and the mantle wedge: A view from the experimentalists. *Geophysical Monograph Series*, *138*, 83–105.

Horodyskyj, U., Lee, C. T. A., & Luffi, P. (2009). Geochemical evidence for exhumation of eclogite via serpentinite channels in ocean-continent subduction zones. *Geosphere*, *5*(5), 426–438. https://doi.org/10.1130/GES00502.1

Huismans, R. S., Podladchikov, Y. Y., & Cloetingh, S. (2001). Transition from passive to active rifting: Relative importance of asthenospheric doming and passive extension of the lithosphere. *Journal of Geophysical Research*, *106*(B6), 11271–11291. https://doi.org/10.1029/2000jb900424

Husson, L., Brun, J. P., Yamato, P., & Faccenna, C. (2010). Episodic slab rollback fosters exhumation of HP-UHP rocks. *Geophysical Journal of the Royal Astronomical Society*, *179*(3), 1292–1300. https://doi.org/10.1111/j.1365-246x.2009.04372.x

Jolivet, L., Faccenna, C., Goffé, B., Burov, E., & Agard, P. (2003). Subduction tectonics and exhumation of high-pressure metamorphic rocks in the Mediterranean orogens. *American Journal of Science*, *303*(5), 353–409. https://doi.org/10.2475/ajs.303.5.353

Kaus, B. J. P., Mühlhaus, H., & May, D. A. (2010). A stabilization algorithm for geodynamic numerical simulations with a free surface. *Physics of the Earth and Planetary Interiors*, *181*(1–2), 12–20. https://doi.org/10.1016/j.pepi.2010.04.007

Kaus, B. J. P., Popov, A. A., Baumann, T. S., Pusok, A. E., Bauville, A., Fernandez, N., & Collignon, M. (2016). Forward and inverse modeling of lithospheric deformation on geological timescales. *NIC Series*, *48*, 978–983.

Le Bayon, R., de Capitani, C., & Frey, M. (2006). Modelling phase-assemblage diagrams for magnesian metapelites in the system K2O-FeO-MgO-Al2O3- SiO2-H2O: Geodynamic consequences for the Monte Rosa nappe, Western Alps. *Contributions to Mineralogy and Petrology*, *151*(4), 395–412. https://doi.org/10.1007/s00410-006-0067-6

Li, Z. H. (2014). A review on the numerical geodynamic modeling of continental subduction, collision and exhumation. *Science China Earth Sciences*, *57*(1), 47–69. https://doi.org/10.1007/s11430-013-4696-0

Liao, J., Malusà, M. G., Zhao, L., Baldwin, S. L., Fitzgerald, P. G., & Gerya, T. (2018). Divergent plate motion drives rapid exhumation of (ultra) high pressure rocks. *Earth and Planetary Science Letters*, *491*, 67–80. https://doi.org/10.1016/j.epsl.2018.03.024

Liou, J. G., Ernst, W. G., Zhang, R. Y., Tsujimori, T., & Jahn, B. M. (2009). Ultrahigh-pressure minerals and metamorphic terranes–the view from China. *Journal of Asian Earth Sciences*, *35*(3–4), 199–231. https://doi.org/10.1016/j.jseaes.2008.10.012

Liou, J. G., Zhang, R. Y., Eide, E. A., Maruyama, S., Wang, X., & Ernst, W. G. (1996). Metamorphism and tectonics of high-P and ultrahigh-P belts in Dabie–Sulu Regions, eastern central China. In A. Yin & T. M. Harrison, (Eds.), *The tectonic evolution of Asia* (pp. 300–343). Cambridge University Press.

Luisier, C., Baumgartner, L., Schmalholz, S. M., Siron, G., & Vennemann, T. (2019). Metamorphic pressure variation in a coherent Alpine nappe challenges lithostatic pressure paradigm. *Nature Communications*, *10*(1), 4734. https://doi.org/10.1038/s41467-019-12727-z

Luo, Y., Xu, Y., & Yang, Y. (2012). Crustal structure beneath the Dabie orogenic belt from ambient noise tomography. *Earth and Planetary Science Letters*, *313*, 12–22. https://doi.org/10.1016/j.epsl.2011.11.004

Maffeis, A., Petroccia, A., Nerone, S., Caso, F., Corno, A., Bonazzi, M., et al. (2025). Filling the gap in the UHP metamorphic record of the Liguro-Piemont Lower unit: Insights on fluid-mediated formation of atoll garnets. *Lithos*, *498–499*, 107981. https://doi.org/10.1016/j.lithos.2025.107981

Malusà, M. G., Anfinson, O. A., Dafov, L. N., & Stockli, D. F. (2016). Tracking Adria indentation beneath the Alps by detrital zircon U-Pb geochronology: Implications for the Oligocene–Miocene dynamics of the Adriatic microplate. *Geology*, *44*(2), 155–158. https://doi.org/10.1130/g37407.1

Malusà, M. G., Faccenna, C., Baldwin, S. L., Fitzgerald, P. G., Rossetti, F., Balestrieri, M. L., et al. (2015). Contrasting styles of (U)HP rock exhumation along the Cenozoic Adria-Europe plate boundary (Western Alps, Calabria, Corsica). *Geochemistry, Geophysics, Geosystems*, *16*(6), 1786–1824. https://doi.org/10.1002/2015GC005767

Malusà, M. G., Faccenna, C., Garzanti, E., & Polino, R. (2011). Divergence in subduction zones and exhumation of high pressure rocks (Eocene Western Alps). *Earth and Planetary Science Letters*, *310*(1–2), 21–32. https://doi.org/10.1016/j.epsl.2011.08.002

Malusà, M. G., & Garzanti, E. (2012). Actualistic snapshot of the early Oligocene Alps: The Alps-Apennines knot disentangled. *Terra Nova*, *24*(1), 1–6. https://doi.org/10.1111/j.1365-3121.2011.01030.x

Malusà, M. G., Guillot, S., Zhao, L., Paul, A., Solarino, S., Dumont, T., et al. (2021). The deep structure of the Alps based on the CIFALPS seismic experiment: A synthesis. *Geochemistry, Geophysics, Geosystems*, *22*(3), e2020GC009466. https://doi.org/10.1029/2020GC009466

Malusà, M. G., Polino, R., & Martin, S. (2005). The Gran San Bernardo nappe in the Aosta valley (western Alps): A composite stack of distinct continental crust units. *Bulletin de la Societe Geologique de France*, *176*(5), 417–431. https://doi.org/10.2113/176.5.417

Manzotti, P., Schiavi, F., Nosenzo, F., Pitra, P., & Ballèvre, M. (2022). A journey towards the forbidden zone: A new cold UHP unit in the Dora-Maira Massif (Western Alps). *Contributions to Mineralogy and Petrology*, *177*(6), 59. https://doi.org/10.1007/s00410-022-01923-8

Monteleone, B. D., Baldwin, S. L., Webb, L. E., Fitzgerald, P. G., Grove, M., & Schmitt, A. (2007). Evidence for late Miocene to Pliocene HP metamorphism in eclogites from the D'Entrecasteaux Islands, SE Papua New Guinea. *Journal of Metamorphic Geology*, *25*(2), 245–265. https://doi.org/10.1111/j.1525-1314.2006.00685.x

Petersen, K. D., & Buck, W. R. (2015). Education, extension, and exhumation of ultrahigh-pressure rocks in metamorphic core complexes due to subduction initiation. *Geochemistry, Geophysics, Geosystems*, *16*(8), 2564–2581. https://doi.org/10.1002/2015gc005847

Popov, A. A., & Kaus, B. J. P. (2025). LaMEM-Lithosphere and Mantle evolution model [Software]. *Zenodo*. Retrieved from https://zenodo.org/records/15524303

Radulescu, I. G., Rubatto, D., Gregory, C., & Compagnoni, R. (2009). The age of HP metamorphism in the Gran Paradiso Massif, Western Alps: A petrological and geochronological study of "silvery micaschists". *Lithos*, *110*(1–4), 95–108. https://doi.org/10.1016/j.lithos.2008.12.008

Raimbourg, H., Jolivet, L., & Leroy, Y. (2007). Consequences of progressive eclogitization on crustal exhumation, a mechanical study. *Geophysical Journal International*, *168*(1), 379–401. https://doi.org/10.1111/j.1365-246X.2006.03130.x

Ranalli, G. (1995). *Rheology of the Earth* (2nd ed.). Chapman & Hall.

Reinecke, T. (1991). Very-high-pressure metamorphism and uplift of coesite-bearing metasediments from the Zermatt-Saas zone, Western Alps. *European Journal of Mineralogy*, *3*(1), 7–17. https://doi.org/10.1127/ejm/3/1/0007

Rubatto, D., & Hermann, J. (2001). Exhumation as fast as subduction? *Geology*, *29*(1), 3–6. https://doi.org/10.1130/0091-7613(2001)029<0003:EAFAS>2.0.CO;2

Sizova, E., Hauzenberger, C. A., Fritz, H., & Gerya, T. (2024). P-T-t evolution of mantle and associated crustal rocks in collisional orogens: Insight from numerical experiments. *Earth-Science Reviews*, *250*(February), 104707. https://doi.org/10.1016/j.earscirev.2024.104707

Solarino, S., Malusà, M. G., Eva, E., Guillot, S., Paul, A., Schwartz, S., et al. (2018). Mantle wedge exhumation beneath the Dora-Maira (U)HP dome unravelled by local earthquake tomography (Western Alps). *Lithos*, *296–299*, 623–636. https://doi.org/10.1016/j.lithos.2017.11.035

Solarino, S., Malusà, M. G., Eva, E., Paul, A., Guillot, S., Pondrelli, S., et al. (2024). Seismic tomography reveals contrasting styles of subduction-channel and mantle-wedge exhumation controlled by upper plate divergent motion. *Gondwana Research*, *136*, 169–182. https://doi.org/10.1016/j.gr.2024.08.016

Starr, P. G., Broadwell, K. S., Dragovic, B., Scambelluri, M., Haws, A. A., Caddick, M. J., et al. (2020). The subduction and exhumation history of the Voltri Ophiolite, Italy: Evaluating exhumation mechanisms for high-pressure metamorphic massifs. *Lithos*, *376–377*, 105767. https://doi.org/10.1016/j.lithos.2020.105767

Taylor, B., Goodliffe, A. M., & Martinez, F. (1999). How continents break up: Insights from Papua New Guinea. *Journal of Geophysical Research*, *104*(B4), 7497–7512. https://doi.org/10.1029/1998jb900115

Turino, V., & Holt, A. (2024). Spatio-temporal variability in slab temperature within dynamic 3-D subduction models. *Geophysical Journal International*, *236*(3), 1484–1498. https://doi.org/10.1093/gji/ggad489

Van Hinsbergen, D. J. J., Mensink, M., Langereis, C. G., Maffione, M., Spalluto, L., Tropeano, M., & Sabato, L. (2014). Did Adria rotate relative to Africa? *Solid Earth*, *5*(2), 611–629. https://doi.org/10.5194/se-5-611-2014

Vaughan-Hammon, J. D., Luisier, C., Baumgartner, L. P., & Schmalholz, S. M. (2021). Peak Alpine metamorphic conditions from staurolite-bearing metapelites in the Monte Rosa nappe (Central European Alps) and geodynamic implications. *Journal of Metamorphic Geology*, *39*(7), 897–917. https://doi.org/10.1111/jmg.12595

Wallace, L. M., Ellis, S., Little, T., Tregoning, P., Palmer, N., Rosa, R., et al. (2014). Continental breakup and UHP rock exhumation in action: GPS results from the Woodlark Rift, Papua New Guinea. *Geochemistry, Geophysics, Geosystems*, *15*(11), 4267–4290. https://doi.org/10.1002/2014gc005458

Wallace, L. M., Stevens, C., Silver, E., McCaffrey, R., Loratung, W., Hasiata, S., et al. (2004). GPS and seismological constraints on active tectonics and arc-continent collision in Papua New Guinea: Implications for mechanics of microplate rotations in a plate boundary zone. *Journal of Geophysical Research*, *109*(5), 1–16. https://doi.org/10.1029/2003JB002481

Wang, E., Meng, Q., Burchfiel, B. C., & Zhang, G. (2003). Mesozoic large-scale lateral extrusion, rotation, and uplift of the Tongbai-Dabie Shan belt in East China. *Geology*, *31*(4), 307–310. https://doi.org/10.1130/0091-7613(2003)031<0307:MLSLER>2.0.CO;2

Wang, X. X. (2025). 3-D modeling of differential exhumation of ultrahigh-pressure metamorphic rocks driven by increasing plate divergence [Dataset]. *figshare*. Retrieved from https://figshare.com/articles/dataset/Data_for_3D-Alps_manuscript/30121378

Wang, X. X., Kaus, B. J. P., Yang, J. F., Wang, K., Li, Y., Chen, L., & Zhao, L. (2021). 3D geodynamic models for HP-UHP Rock exhumation in opposite-dip double subduction-collision systems. *Journal of Geophysical Research: Solid Earth*, *126*(8), e2021JB022326. https://doi.org/10.1029/2021jb022326

Webb, L. E., Baldwin, S. L., Little, T. A., & Fitzgerald, P. G. (2008). Can microplate rotation drive subduction inversion? *Geology*, *36*(10), 823–826. https://doi.org/10.1130/G25134A.1

Yamato, P., & Brun, J. P. (2017). Metamorphic record of catastrophic pressure drops in subduction zones. *Nature Geoscience*, *10*(1), 46–50. https://doi.org/10.1038/ngeo2852

Yamato, P., Burov, E., Agard, P., Le Pourhiet, L., & Jolivet, L. (2008). HP-UHP exhumation during slow continental subduction: Self-consistent thermodynamically and thermomechanically coupled model with application to the Western Alps. *Earth and Planetary Science Letters*, *271*(1–4), 63–74. https://doi.org/10.1016/j.epsl.2008.03.049

Zahorec, P., Papco, J., Pašteka, R., Bielik, M., Bonvalot, S., Braitenberg, C., et al. (2021). The first Pan-Alpine surface-gravity database, a modern compilation that crosses frontiers. *Earth and Planetary Science Letters*, *13*(5), 2165–2209. https://doi.org/10.5194/essd-13-2165-2021

Zhang, L., & Wang, Y. (2020). The exhumation of high- and ultrahigh-pressure metamorphic terranes in subduction zone: Questions and discussions. *Science China Earth Sciences*, *7*(2), 1–16. https://doi.org/10.1007/s11430-020-9579-3

Zhao, L., Malusà, M. G., Yuan, H., Paul, A., Guillot, S., Lu, Y., et al. (2020). Evidence for a serpentinized plate interface favouring continental subduction. *Nature Communications*, *11*(1), 2171. https://doi.org/10.1038/s41467-020-15904-7

Zhao, L., Paul, A., Guillot, S., Solarino, S., Malusà, M. G., Zheng, T. Y., et al. (2015). First seismic evidence for continental subduction beneath the Western Alps. *Geology*, *43*(9), 815–819. https://doi.org/10.1130/G36833.1

Zhao, L., Paul, A., Malusà, M. G., Xu, X., Zheng, T., Solarino, S., et al. (2016). Continuity of the Alpine slab unraveled by high-resolution P wave tomography. *Journal of Geophysical Research: Solid Earth*, *121*(12), 8720–8737. https://doi.org/10.1002/2016JB013310